Microwave Measurement of the Wind Vector over Sea by Airborne Radars

Alexey Nekrasov

Taganrog Institute of Technology of the Southern Federal University
Russia,
Hamburg University of Technology
Germany

1. Introduction

The oceans of the Earth work in concert with the atmosphere to control and regulate the environment. Fed by the sun, the interaction of land, ocean, and atmosphere produces the phenomenon of weather and climate. Only in the past half-century meteorologists have begun to understand weather patterns well enough to produce relatively accurate, although limited, forecasts of future weather patterns. One limitation of predicting future weather is that meteorologists do not adequately know the current weather. An accurate understanding of current conditions over the ocean is required to predict future weather patterns. Until recently, detailed local oceanic weather conditions were available only from sparsely arrayed weather stations, ships along commercial shipping lanes and sparsely distributed oceans buoys (Long, et al, 1976).

The development of satellite and airborne remote sensing has improved the situation significantly. Satellite remote sensing has demonstrated its potential to provide measurements of weather conditions on a global scale as well as airborne remote sensing on a local scale. Measurements of surface wind vector and wave height are assimilated into regional and global numerical weather and wave models, thereby extending and improving our ability to predict future weather patterns and sea/ocean surface conditions on many scales.

A pilot also needs operational information about wind over sea as well as wave height to provide safety of hydroplane landing on water.

Many researchers solve the problem of remote measuring of the wind vector over sea actively (Moore & Fung, 1979), (Melnik, 1980), (Chelton & McCabe, 1985), (Feindt, et al, 1986), (Masuko, et al, 1986), (Wismann, 1989), (Hildebrand, 1994), (Carswell, et al, 1994). On the global scale, the information about sea waves and wind, in general, could be obtained from a satellite using active microwave instruments: Scatterometer, Synthetic Aperture Radar (SAR) and Radar Altimeter. However, for the local numerical weather and wave

models as well as for a pilot on a hydroplane to make a landing decision, the local data about wave height, wind speed and direction are required.

Research on microwave backscatter by the sea surface has shown that the use of a scatterometer, radar designed for measuring the surface scatter characteristics, allows for an estimation of sea surface wind vector because the normalized radar cross section (NRCS) of the sea surface depends on the wind speed and direction. Based on experimental data and scattering theory, a significant number of empirical and theoretical backscatter models and algorithms for estimation of the sea wind speed and direction from satellite and airplane have been proposed (Long, et al, 1976), (Moore & Fung, 1979), (Melnik, 1980), (Chelton & McCabe, 1985), (Masuko, et al, 1986), (Wismann, 1989), (Hildebrand, 1994), (Carswell, et al, 1994), (Wentz, et al, 1984), (Young, (1993), (Romeiser, et al, 1994). The accuracy of the wind direction measurement is ±20°, and the accuracy of the wind speed measurement is ±2 m/s in the wind speed range 3–24 m/s.

SAR provides an image of the roughness distribution on the sea surface with large dynamic range, high accuracy, and high resolution. Retrieval of wind information from SAR images provides a useful complement to support traditional wind observations (Du, et al, 2002). Wind direction estimation amounts to measuring the orientation of boundary-layer rolls in the SAR image, which are often visible as image streaks. The sea surface wind direction (to within a 180° direction ambiguity) is assumed to lie essentially parallel to the roll or image-streak orientation. Wind speed estimation from SAR images is usually based on a scatterometer wind retrieval models. This approach requires a well-calibrated SAR image. The wind direction estimated from the European remote sensing satellite (ERS-1) SAR images is within a root mean square (RMS) error of ±19° of in situ observations, which in turn results in an RMS wind speed error of ±1.2 m/s (Wackerman, et al, 1996).

The radar altimeter also provides the information on the sea wind speed, which can be determined from the intensity of the backscattered return pulse, and on the sea wave height, which can be deduced from the return pulse shape. At moderate winds (3–12 m/s), the wind speed can be measured by the altimeter with an accuracy of about ±2 m/s. The typical accuracy of radar altimeter measurements of the significant wave height is of the order of ±0.5 m (or 10 %, whichever is higher) for wave heights between 1 and 20 m (Komen, et al, 1994). Unfortunately, altimeter wind measurements yield wind velocity magnitude only, and do not provide information on wind direction.

Mostly narrow-beam antennas are applied for such wind measurement. Unfortunately, a microwave narrow-beam antenna has considerable size at Ku-, X- and C-bands that hampers its placing on flying apparatus. Therefore, a better way needs to be found.

At least two ways can be proposed. The first way is to apply the airborne scatterometers with wide-beam antennas as it can lead to the reduction in the antenna size. The second way is to use the modified conventional navigation instruments of flying apparatus in a scatterometer mode, which is more preferable.

From that point of view, the promising navigation instruments are the airborne radar altimeter (ARA), the Doppler navigation system (DNS) and the airborne weather radar (AWR). So, the principles of recovering the sea surface wind speed and direction, using those navigation instruments are discussed in this chapter.

2. Principle of Near-Surface Wind Vector Estimation

Radar backscatter from the sea surface varies considerably with incidence angle (Hildebrand, 1994). Near nadir is a region of quasi-specular return with a maximum of NRCS that falls with increasing the angle of incidence. Between incident angles of about 20° and 70°, the NRCS falls smoothly in a so-called "plateau" region. For middle incident angles, microwave radar backscatter is predominantly due to the presence of capillary-gravity wavelets, which are superimposed on large gravity waves on the sea surface. Small-scale sea waves of a length approximately one half the radar wavelength are in Bragg resonance with an incident electromagnetic wave. At incidence angles greater than about 70° is the "shadow" region in which NRCS falls dramatically, due to the shadowing effect of waves closer to the radar blocking waves further away.

The wind blowing over sea modifies the surface backscatter properties. These depend on wind speed and direction. Wind speed U can be determined by a scatterometer because a stronger wind will produce a larger NRCS $\sigma^\circ(U, \theta, \alpha)$ at the middle incidence angle θ and a smaller NRCS at the small (near nadir) incidence angle. Wind direction can also be inferred because the NRCS varies as a function of the azimuth illumination angle α relative to the up-wind direction (Spencer & Graf, 1997).

To extract the wind vector from NRCS measurements, the relationship between the NRCS and near-surface wind, called the "geophysical model function", must be known. Scatterometer experiments have shown that the NRCS model function for middle incidence angles is of the widely used form (Spencer & Graf, 1997)

$$\sigma^\circ(U, \theta, \alpha) = A(U, \theta) + B(U, \theta)\cos\alpha + C(U, \theta)\cos(2\alpha), \qquad (1)$$

where $A(U, \theta)$, $B(U, \theta)$ and $C(U, \theta)$ are the Fourier terms that depend on sea surface wind speed and incidence angle, $A(U, \theta) = a_0(\theta)U^{\gamma_0(\theta)}$, $B(U, \theta) = a_1(\theta)U^{\gamma_1(\theta)}$, and $C(U, \theta) = a_2(\theta)U^{\gamma_2(\theta)}$; $a_0(\theta)$, $a_1(\theta)$, $a_2(\theta)$, $\gamma_0(\theta)$, $\gamma_1(\theta)$ and $\gamma_2(\theta)$ are the coefficients dependent on the incidence angle.

As we can see from (1), an NRCS azimuth curve has two maxima and two minima. The main maximum is located in the up-wind direction, the second maximum corresponds to the down-wind direction, and two minima are in cross-wind directions displaced slightly to the second maximum. With increase of the incidence angle, the difference between two maxima and the difference between maxima and minima become so significant (especially at middle incidence angles) that this feature can be used for retrieval of the wind direction over water (Ulaby, et al, 1982).

In the general case, the problem of estimating the sea surface wind navigational direction ψ_w consists in defining the main maximum of a curve of the reflected signal intensity (azimuth of the main maximum of the NRCS $\psi_{\sigma^\circ_{max}}$)

$$\psi_w = \psi_{\sigma^\circ_{max}} \pm 180^\circ, \qquad (2)$$

and the problem of deriving the sea surface wind speed consists in determination of a reflected signal intensity value from the up-wind direction or from some or all of the azimuth directions. The azimuth NRCS curve can be obtained using the circle track flight for a scatterometer with an inclined one-beam fixed-position antenna or the rectilinear track flight for a scatterometer with a rotating antenna (Masuko, et al, 1986), (Wismann, 1989), (Carswell, et al, 1994).

Also, the wind speed over sea can be measured by a scatterometer with a nadir-looking antenna (altimeter) using, for instance, the following NRCS model function at zero incident angle $\sigma^\circ(U,0^\circ)$ (Chelton & McCabe, 1985).

$$\sigma^\circ(U,0^\circ)[dB] = 10\left(G_1 + G_2 \log_{10} U_{19.5}\right), \tag{3}$$

where G_1 and G_2 are the parameters, $G_1 = 1.502$, $G_2 = -0.468$; $U_{19.5}$ is the wind speed at 19.5 m above the sea surface. A comparison of altimeter wind speed algorithms together with (3) is represented in (Schöne & Eickschen, 2000).

Thus, the scatterometer having an antenna with inclined beams provides the information on both the wind speed over sea and the wind direction, and the scatterometer with a nadir-looking antenna allows estimating only the sea surface wind speed and provides no information on the wind direction.

3. Wind Vector Measurement Using an Airborne Radar Altimeter

3.1 Airborne Radar Altimeter

The basic function of the ARA is to provide terrain clearance or altitude with respect to the ground level directly beneath the aircraft. The ARA may also provide vertical rate of climb or descent and selectable low altitude warning (Kayton & Fried, 1997).

Altimeters perform the basic function of any range measuring radar. A modulated signal is transmitted toward the ground. The modulation provides a time reference to which the reflected return signal can be reflected, thereby providing radar-range or time delay and therefore altitude. The ground represents an extended target, as opposed to a point target, resulting in the delay path extending from a point directly beneath the aircraft out to the edge of antenna beam. Furthermore, the beam width of a dedicated radar altimeter antenna must be wide enough to accommodate normal roll-and-pitch angles of the aircraft, resulting in a significant variation in return delay.

The ARA is constructed as FM-CW or pulsed radar. The frequency band of 4.2 to 4.4 GHz is assigned to the ARA. The frequency band is high enough to result in reasonably small sized antennas to produce a 40° to 50° beam but is sufficiently low so that rain attenuation and backscatter from rain have no significant range limiting effects. Typical installations include a pair of small microstrip antennas for transmit and receive functions (Kayton & Fried, 1997).

3.2 Beam Sharpening

As the ARA has a widebeam antenna and wind measurements are performed with the antennas having comparatively narrow beams (beamwidth of $4^\circ - 10^\circ$), to apply the ARA for wind vector estimation the beam sharpening technologies should be used.

Lately, to sharpen the effective antenna beams of real-aperture radars avoiding the size enlargement of their antennas, Doppler discrimination along with range discrimination have been employed. An example of application of such a simultaneous range Doppler discrimination technique is the conically scanning pencil-beam scatterometer performing wind retrieval (Spencer, et al, 2000a). When simultaneous range Doppler processing is used, the resolution cell is delineated by the iso-Doppler and iso-range lines projected on the surface, where the spacing between the lines is the achievable Doppler or range resolution respectively. As the beam scans, the azimuth resolution is the best at the side-looking locations and is the coarsest at the forward and afterward locations. A conceptual description of such a scatterometer has been described in (Spencer, et al, 2000b).

Another example of employing the simultaneous range Doppler discrimination technique is the delay Doppler radar altimeter developed at the Applied Physics Laboratory of the Johns Hopkins University (Raney, 1998). The delay Doppler altimeter uses coherent processing over a block of received returns to estimate the Doppler frequency modulation imposed on the signals by the forward motion of the altimeter. Doppler analysis of the data allows estimating their along-track positions relative to the position of the altimeter. It follows that the along-track dimension of the signal data and the cross-track (range or time delay) dimensions are separable. In contrast to the response of a conventional altimeter having only one independent variable (time delay), the delay Doppler altimeter response has two independent variables: along-track position (functionally related to Doppler frequency) and cross-track position (functionally related to time delay). After delay Doppler processing, these two variables describe an orthonormal data grid. With this data space in mind, delay Doppler processing may be interpreted as an operation that flattens the radiating field in along-track direction. Unfortunately, a cross-track ambiguity takes place under measurements, as there are two possible sources of reflections (one from the left side and another from the right side), which have a given time delay at any given Doppler frequency (Raney, 1998).

Recently, the sensitivity of signals from the Global Positioning System (GPS) to propagation effects was found to be useful for measurements of surface roughness characteristics from which wave height, wind speed, and direction could be determined. The Delay Mapping Receiver (DMR) was designed, and a number of airborne experiments were completed. The DMR includes two low-gain (wide-beam) L-band antennas: a zenith mounted right-hand circular polarized antenna, and a nadir mounted left-hand circular polarized (LHCP) antenna. It is assumed that a downward-looking LHCP antenna intercepts only the scattered signal and is insensitive to the direct signal. By combining code-range and Doppler measurements, the receiver distinguished particular patches of the ocean surface illuminated by GPS signal that, in fact, is the delay Doppler spatial selection. The estimated wind speed using surface-reflected GPS data collected at a variety of wind speed conditions showed an overall agreement better than 2 m/s with data obtained from nearby buoy data and independent wind speed measurements derived from satellite observations. Wind direction agreement with QuikSCAT measurements appeared to be at the 30° degree level (Komjathy, et al, 2001), (Komjathy, et al, 2000).

3.3 Wind Vector Estimation Using an Airborne Radar Altimeter with the Antenna Forming the Circle Footprint

As the radar altimeter and the scatterometer are required on board of an amphibious airplane, their measurements should be integrated in a single instrument. One of the ways

of such integration is to use a short-pulse wide-beam nadir-looking radar, like an airborne Wind-Wave Radar (Hammond, et al, 1977), but with additional Doppler filters. Here, only a short-pulse scatterometer mode of estimating the wind vector by such an airborne altimeter is considered (Nekrassov, 2003).

Let a flying apparatus equipped with a scatterometer (altimeter) having a nadir-looking wide-beam antenna make a horizontal rectilinear flight with the speed V at some altitude H above the mean sea surface, the antenna have the same beamwidth θ_a in both the vertical and horizontal planes, forming a glistening zone on the sea surface, and then transmit a short pulse of duration τ at some time $t = 0$ (Fig. 1). If the surface is (quasi-) flat, the first signal return, from the nadir point, occurs at time $t_0 = 2H/c$, where c is the speed of light. The trailing edge of the pulse undergoes the same interactions as the leading edge but delayed in time by τ. The last energy is received from nadir at time $t_0 + \tau$, and the angle for the pulse-limited footprint is $\theta_p = \sqrt{c\tau/H}$. For larger values of time, an annulus is illuminated. The angular incident resolution $\Delta\theta$ is the poorest at nadir, and it improves rapidly with the time from the nadir point.
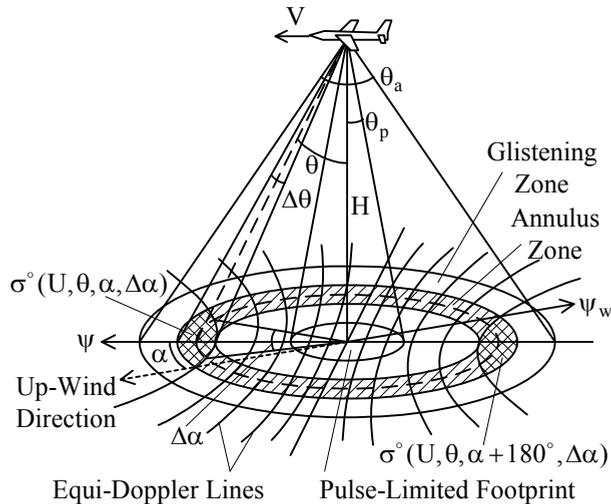

Fig. 1. Two-cell geometry of wind vector measurement by the ARA with the antenna forming a circle footprint

Let the NRCS model function for middle incident angles (annulus zone) be of the form (1) and the NRCS model function for the pulse-limited footprint be of the form (3). Then, the following algorithm to estimate the wind vector over the sea surface can be proposed.

The wind speed can be obtained by means of nadir measurement, for instance, from (3) and converted to a height of measurement of 10 m ($U_{10} = U$), which is mostly used today; for a neutral stability wind profile using the following expression (Jackson, et al, 1992)

$$U_{10} = 0.93 U_{19.5} = 0.93 \cdot 10^{[\log_{10} \sigma^\circ(U,0^\circ) - G_1]/G_2} , \tag{4}$$

or using (1), the average azimuthally integrated NRCS obtained from the annulus zone $\sigma_{an}^{\circ}(U,\theta)$ can be represented in the following form (Nekrassov, 2002)

$$\sigma_{an}^{\circ}(U,\theta) = \frac{1}{2\pi}\int_{0}^{2\pi}\sigma^{\circ}(U,\theta,\alpha)d\alpha = A(U,\theta) \tag{5}$$

and then the wind speed can be found from the following equation

$$U = \left(\frac{A(U,\theta)}{a_0(\theta)}\right)^{1/\gamma_0(\theta)} = \left(\frac{\sigma_{an}^{\circ}(U,\theta)}{a_0(\theta)}\right)^{1/\gamma_0(\theta)}. \tag{6}$$

This method of wind speed estimation allows averaging the power reflected from whole annulus area. However, NRSC values from essentially different athimuthal directions are required to derive a wind direction.

It is necessary to note that the dependence of measured NRCS value on the angular size of a pulse-limited footprint should be taken into account, if the narrow-beam NRCS model function is used. Therefore, the nadir NRCS data obtained by an altimeter having a nadir-looking wide-beam antenna should be corrected in case of a pulse-limited footprint angular size is over approximately $5^{\circ} - 6^{\circ}$ (Nekrassov, 2001).

Now assume that narrow enough Doppler zones could be provided by means of Doppler filtering (Fig. 1). Then, the intersection of an annulus with a Doppler zone would form a spatial cell that discriminates the signal scattered back from the appropriate area of the annulus in the azimuthal direction. Employing Doppler filtering, which provides the azimuthal selection under the measurements with the azimuth resolution (azimuth angular size of a cell) $\Delta\alpha$ in the directions of 0° and 180° relative to the flying apparatus' course as represented by Fig. 1, the wind direction can be derived. To provide the required azimuth angular sizes of the cells, the frequency limits of the fore-Doppler filter $F_{D1.f}$ and $F_{D2.f}$ and of the aft-Doppler filter $F_{D1.a}$ and $F_{D2.a}$ (relative to the zero-Doppler frequency shift) should be as follows

$$F_{D1.f} = -F_{D1.a} = \frac{2V}{\lambda}\sin\left(\theta - \frac{\Delta\theta}{2}\right),$$

$$F_{D2.f} = -F_{D2.a} = \frac{2V}{\lambda}\sin\left(\theta + \frac{\Delta\theta}{2}\right), \tag{7}$$

where λ is the radar wavelength.

At low speed of flight the Doppler effect is not so considerable as at higher speed of flight, and so such locations of the selected cells allows to use the maximum Doppler shifts available. Unfortunately, the coarsest azimuth resolution

$$\Delta\alpha = 2\arccos\left(\frac{\sin(\theta - \Delta\theta)}{\sin\theta}\right) \tag{8}$$

takes place in that case, and the NRCS model function $\sigma^\circ(U, \theta, \alpha, \Delta\alpha)$, which considers the azimuth angular size of a cell, should be used.

$$\sigma^\circ(U, \theta, \alpha, \Delta\alpha) = \frac{1}{\Delta\alpha} \int\limits_{\alpha - 0.5\Delta\alpha}^{\alpha + 0.5\Delta\alpha} \sigma^\circ(U, \theta, \alpha') d\alpha'$$
$$= A(U, \theta) + k_1(\Delta\alpha)B(U, \theta)\cos\alpha + k_2(\Delta\alpha)C(U, \theta)\cos(2\alpha), \qquad (9)$$

where $k_1(\Delta\alpha)$ and $k_2(\Delta\alpha)$ are the coefficients dependent on the azimuth angular size of a cell

$$k_1(\Delta\alpha) = \frac{2\sin(0.5\Delta\alpha)}{\Delta\alpha},$$
$$k_2(\Delta\alpha) = \frac{\sin\Delta\alpha}{\Delta\alpha}. \qquad (10)$$

Let $\sigma^\circ(U, \theta, \alpha, \Delta\alpha)$, and $\sigma^\circ(U, \theta, \alpha + 180^\circ, \Delta\alpha)$ be the NRCS obtained with the fore-Doppler and aft-Doppler filters from the cells corresponding to the maximum value of the Doppler shift (Fig. 1). Then, the speed of wind can be found from (6), and two possible wind directions $\psi_{w.1,2}$ can be found as the following

$$\psi_{w.1,2} = \psi - \alpha_{1,2} \pm 180^\circ, \qquad (11)$$

where $\alpha_{1,2}$ are two possible up-wind directions

$$\alpha_{1,2} = \pm\arccos\left(\frac{\sigma^\circ(U, \theta, \alpha, \Delta\alpha) - \sigma^\circ(U, \theta, \alpha + 180^\circ, \Delta\alpha)}{2k_1(\Delta\alpha)B(U, \theta)}\right). \qquad (12)$$

Unfortunately, an ambiguity of the wind direction takes place in the measurement. Nevertheless, this ambiguity can be eliminated by recurring measurement after 45° change of the flying apparatus' course. The nearest wind directions of pairs of wind directions measured before and after course changing will give the true wind direction.

3.4 Wind Vector Estimation Using an Airborne Radar Altimeter with the Antenna Forming the Ellipse Footprint

To eliminate need of measurements with two different courses of flight under estimation of the sea surface wind speed and direction by the ARA, a modified beam shape forming the ellipse footprints should be used (Nekrasov, 2008a).

Let the antenna beam is wide enough, then two annulus zones at incidence angles θ_1 and θ_2 could be formed as shown by Fig. 2. They will have angular incidence widths $\Delta\theta_1$ and $\Delta\theta_2$ respectively. Now, let the altimeter antenna form an ellipse footprint so that the longer axis

of the footprint is rotated by 45° from the horizontal projection of the longitudinal axis of a flying apparatus as shown in Fig. 3.
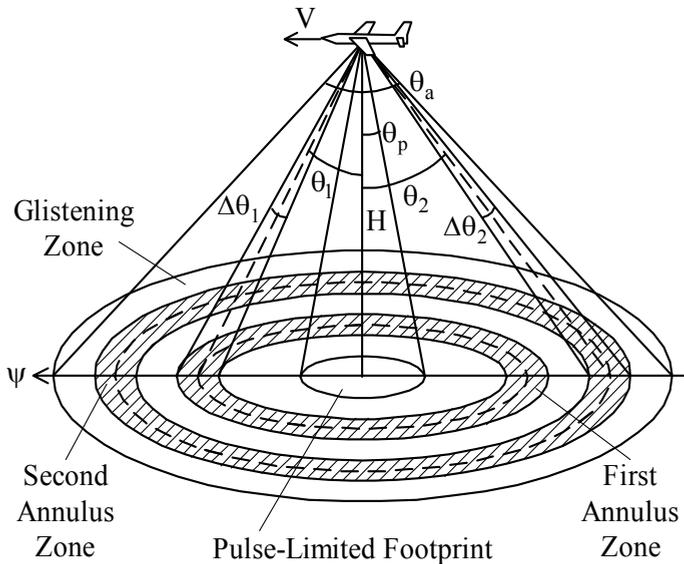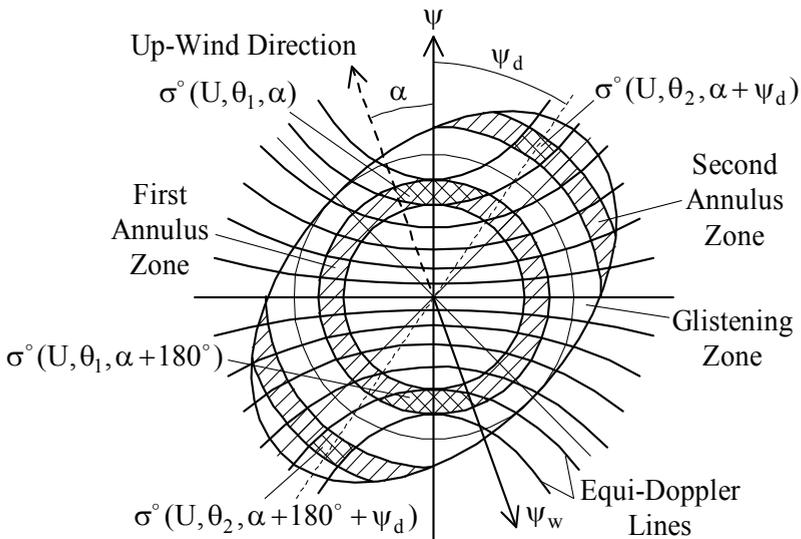
Fig. 2. Forming the annulus zones

Fig. 3. Geometry of wind vector measurement by ARA having the antenna with the different beamwidth in the vertical and horizontal planes, forming the ellipse footprint, when the longer axis of the footprint is rotated by 45° from the horizontal projection of the longitudinal axis of a flying apparatus

Then, two annulus zones at incidence angles θ_1 and θ_2 ($\theta_1 < \theta_{a.h} < \theta_2 < \theta_{a.v}$) could be formed, and the range Doppler selection can facilitate the identification of cells with the NRCS $\sigma^\circ(U, \theta_1, \alpha)$ and $\sigma^\circ(U, \theta_1, \alpha + 180^\circ)$ corresponding the azimuth directions α and $\alpha + 180^\circ$ from the first annulus, and the identification of cells with the NRCS $\sigma^\circ(U, \theta_2, \alpha + \psi_d)$ and $\sigma^\circ(U, \theta_2, \alpha + 180^\circ + \psi_d)$ corresponding the azimuth directions $\alpha + \psi_d$ and $\alpha + 180^\circ + \psi_d$ from the second annulus.

To provide the required azimuth angular sizes of cells of the first annulus $\Delta\alpha_1$ and the second annulus $\Delta\alpha_2$, as shown in Fig. 4, the frequency limits of the fore-Doppler filter $F_{D1.f}$ and $F_{D2.f}$, and of the aft-Doppler filter $F_{D1.a}$ and $F_{D2.a}$ (relative to the zero-Doppler frequency shift) should be as follows

$$F_{D1.f} = -F_{D1.a} = \frac{2V}{\lambda} \sin\left(\theta_1 - \frac{\Delta\theta_1}{2}\right),$$

$$F_{D2.f} = -F_{D2.a} = \frac{2V}{\lambda} \sin\left(\theta_1 + \frac{\Delta\theta_1}{2}\right); \tag{13}$$

$$F_{D1.f} = -F_{D1.a} = \frac{2V}{\lambda} \sin\theta_2 \cos\left(\psi_d + \frac{\Delta\alpha_2}{2}\right),$$

$$F_{D2.f} = -F_{D2.a} = \frac{2V}{\lambda} \sin\theta_2 \cos\left(\psi_d - \frac{\Delta\alpha_2}{2}\right). \tag{14}$$
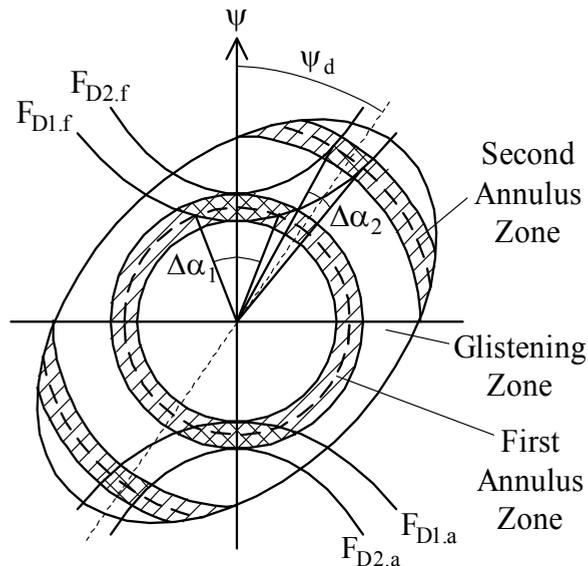

Fig. 4. Forming the selected cells and their angular sizes in horizontal plane

The azimuth angular size of cells of the first annulus is

$$\Delta\alpha_1 = 2\arccos\left(\frac{\sin(\theta_1 - \Delta\theta_1)}{\sin\theta_1}\right).$$
(15)

From (13) and (14), we obtain the azimuth location of cells of the second annulus ψ_d, $180° + \psi_d$, and their angular size in the horizontal plane

$$\psi_d = 0.5\left[\arccos\left(\frac{\sin(\theta_1 - 0.5\Delta\theta_1)}{\sin\theta_2}\right) + \arccos\left(\frac{\sin(\theta_1 + 0.5\Delta\theta_1)}{\sin\theta_2}\right)\right],$$

$$\Delta\alpha_2 = \arccos\left(\frac{\sin(\theta_1 - 0.5\Delta\theta_1)}{\sin\theta_2}\right) - \arccos\left(\frac{\sin(\theta_1 + 0.5\Delta\theta_1)}{\sin\theta_2}\right).$$
(16)

The speed of wind can be found from (6). Two possible up-wind directions $\alpha_{1an.1,2}$ can be found from the NRCS values obtained from cells of the first annulus, and another two possible up-wind directions $\alpha_{2an.1,2}$ can be found from the NRCS values obtained from cells of the second annulus (Nekrasov, 2007)

$$\alpha_{1an.1,2} = \pm\arccos\left(\frac{\sigma°(U,\theta_1,\alpha) - \sigma°(U,\theta_1,\alpha+180°)}{2k_1(\Delta\alpha_1)B(U,\theta_1)}\right),$$

$$\alpha_{2an.1,2} = \pm\arccos\left(\frac{\sigma°(U,\theta_2,\alpha+\psi_d) - \sigma°(U,\theta_2,\alpha+180°+\psi_d)}{2k_1(\Delta\alpha_2)B(U,\theta_2)}\right).$$
(17)

The nearest up-wind directions of pairs of the up-wind directions obtained (one from $\alpha_{1an.1,2}$ and one from $\alpha_{2an.1,2}$) will give the true up-wind direction α, and then, the navigational direction of wind can be found

$$\psi_w = \psi - \alpha \pm 180°.$$
(18)

3.5 Conclusion to Wind Vector Estimation Using an Airborne Radar Altimeter

The study has shown that the wind vector over sea can be measured by means of an ARA employed as a nadir-looking wide-beam short-pulse scatterometer in conjunction with Doppler filtering. Such a measuring instrument should be equipped with two additional Doppler filters (a fore-Doppler filter and an aft-Doppler filter) to provide the spatial selection under the wind measurements.

For the two-cell geometry of wind vector estimation, when the spatially selected cells are located in the directions of 0° and 180° relative to the flying apparatus' course, an ambiguity of the wind direction appears in the measurement. Nevertheless, to find the true wind direction, a recurring measurement after 45° change of the flying apparatus' course is required. The nearest wind directions of pairs of wind directions obtained before and after

course changing will give the true wind direction. To avoid such inconvenience under estimation of the sea surface wind speed and direction by the ARA, a modified beam shape forming the ellipse footprints should be used.

Such an altimeter should operate at a Ku-band (or at least at a C-band) using a horizontal transmit and receive polarization. A lower radar wavelength provides Doppler selection at a lower speed of flight, and at the Ku-band, the upwind/downwind and upwind/crosswind differences in the NRCS values at middle incidence angles (for wind speed of 3 to 24 m/s) are greater than at the lower bands. Horizontal transmit and receive polarizations provide greater upwind/downwind differences in the NRCS values at middle incidence angles than the vertical polarizations. Incidence angle of the second annulus zone should tend to 45°, and the incidence angle of the first annulus zone should be no less than 20°. The antenna should have different beamwidths in the vertical and horizontal planes ($\theta_{a.v} > \theta_{a.h}$) and form the ellipse footprint so that the longer axis of the footprint is rotated by approximately 45° from the horizontal projection of the longitudinal axis of a flying apparatus. It is desirable that the antenna is installed so that the longer axis of the ellipse footprint coincides with the azimuth locations of cells of the second annulus in operating regime.

4. Doppler Navigation System Application for Estimation of the Wind Speed and Direction

4.1 Doppler Navigation System

DNS is the self-contained radar system that utilizes the Doppler effect (Doppler radar) for measuring the ground speed and drift angle of flying apparatus and accomplishes its dead-reckoning navigation (Sosnovskiy & Khaymovich, 1987). The internationally authorized frequency band of 13.25 to 13.4 GHz has been allocated for airborne Doppler navigation radar. A center frequency of 13.325 GHz of the band corresponds to a wave length of 2.25 cm. This frequency represents a good compromise between too low a frequency, resulting in low-velocity sensitivity and large aircraft antenna size and beam widths, and too high a frequency, resulting in excessive absorption and backscattering effects of the atmosphere and precipitation. (Earlier Doppler radars operated in two somewhat lower frequency bands, i.e., centered at 8.8 and 9.8 GHz, respectively, but now these bands are no longer used for stand-alone Doppler radars.) (Kayton & Fried, 1997).

Measurement of the wind vector and drift angle of flying apparatus is based on change of a Doppler frequency of the signal reflected from the underlying surface, depending on a spatial position of an antenna beam. Usually, an antenna of the DNS has three beams (λ-configuration; beams 1, 2, and 3) or four beams (x-configuration; beams 1, 2, 3, and 4) located in space as represented in Fig. 5. An effective antenna beamwidth is of 3° to 10° (Kolchinskiy, et al, 1975). Power reasons (DNS should operates over water as well as over land) and sensitivity of the DNS to velocity influence a choice of a mounting angle of a beam axis in the vertical plane θ_0.

Fig. 6 shows curves of the NRCS versus incidence angle for radar system operating in the frequency band (Ke-band) currently assigned to Doppler navigation radar (Kayton & Fried, 1997). It is seen from the curves that for most types of terrain the NRCS decreases slowly with increase of the beam incidence angle. However, for water surfaces, the NRCS falls radically as the incidence angle increases and assumes different values for different conditions of sea state or water roughness. For the typical Doppler-radar incidence angles of

15° to 30° (Kolchinskiy, et al, 1975), the NRCS is considerably smaller for most sea states than for land and decreases markedly for the smoother sea state. Therefore, a conservative Doppler-radar design is based on an NRCS for the smoothest sea state over which the aircraft is expected to navigate. (Very smooth sea states are relatively rare).

There are two basic antenna system concepts used for drift angle measurement. These are the fixed-antenna system, which is used in most modern systems, and the track-stabilized (roll-and-pitch-stabilized) antenna system. For physically roll-and-pitch-stabilized antenna systems, the value of an incidence angle remains essentially constant and equal to the chosen design value. For fixed-antenna system, a conservative design is based on the NRCS and range for the largest incidence angle that would be expected for the largest combination of pitch and roll angles of the aircraft (Kayton & Fried, 1997).
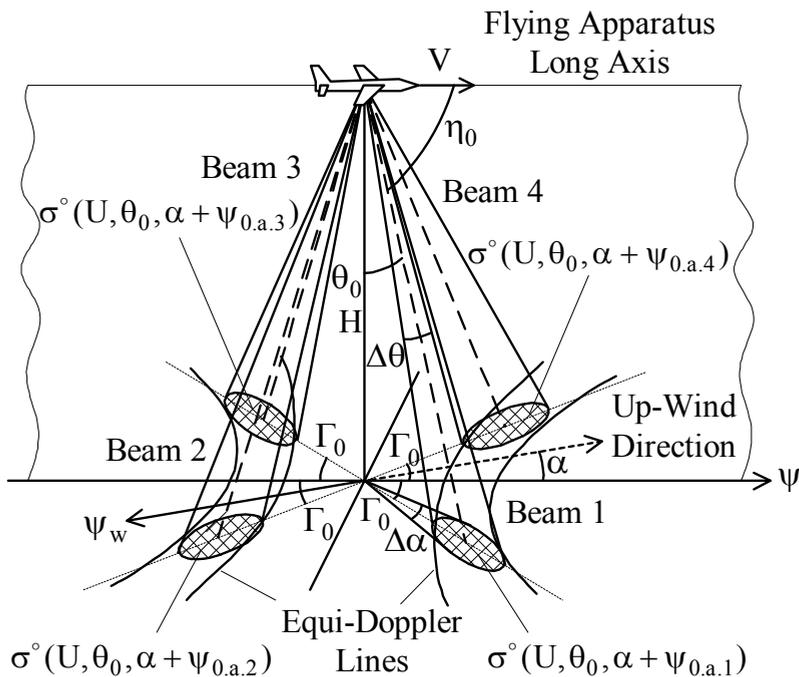
Fig. 5. Typical spatial location of the DNS beams: λ-configuration (beams 1, 2, and 3) and x-configuration (beams 1, 2, 3, and 4)

The choice of a mounting angle of a beam axis in the inclined plane η_0 (nominal angle between antenna longitudinal axis and central beam direction) represents a compromise between high sensitivity to velocity and over-water accuracy, which increases with smaller mounting angles of a beam axis in the inclined plane, and high signal return over water, which increases for larger mounting angles of a beam axis in the inclined plane. Most equipments use a mounting angle of a beam axis in the inclined plane of somewhere between 65° and 80° (Kayton & Fried, 1997). The choice of a mounting angle of a beam axis in the horizontal plane Γ_0 depends on the desired sensitivity to drift, which tends to increase

with increasing that mounting angle. For the typical Doppler-radar, mounting angles of a beam axis in the horizontal plane are of 15° to 45° (Kolchinskiy, et al, 1975).

The relationship among those mounting angles is (Kayton & Fried, 1997)

$$\cos \eta_0 = \cos \Gamma_0 \cos \theta_0 . \tag{19}$$

The mounting angle of a beam axis in the horizontal plane should satisfy the following condition $\Gamma_0 > \beta_{dr.max}$, where $\beta_{dr.max}$ is the maximum possible drift angle (Sosnovskiy & Khaymovich, 1987). The mounting angle of a beam axis in the inclined plane is defined by requirements to the width of a Doppler spectrum of the reflected signal Δf_D, which depends on the effective antenna beamwidth in the inclined plane $\theta_{a.incl}$; $\theta_{a.incl} \approx 5°$ for DNS. The relative width of a Doppler spectrum $\Delta f_D / F_D$ is given by (Davydov, et al, (1977)

$$\frac{\Delta f_D}{F_D} = \frac{\theta_{a.incl}}{\sqrt{2}} \tan \eta_0 , \tag{20}$$

where F_D is the Doppler frequency, $F_D = \dfrac{2V_g}{\lambda} \cos \eta_0$, V_g is the aircraft velocity relative to the ground. To perform high accuracy measurements with the DNS, the following condition should be provided (Davydov, et al, (1977)

$$\frac{\Delta f_D}{F_D} \leq 0.1 \div 0.2 . \tag{21}$$

Thus, from (20) and (21), the mounting angle of a beam axis in the inclined plane should satisfy the following condition

$$\eta_0 \leq \arctan \left[(0.1 \div 0.2) \frac{\sqrt{2}}{\theta_{a.incl}} \right] . \tag{22}$$

From (22), assuming that the effective antenna beamwidth in the inclined plane is typical and equal to 5°, the condition of choice the mounting angle of a beam axis in the inclined plane is

$$\eta_0 \leq 58.3° \div 72.2° . \tag{23}$$

Then, using (19), the areas of admissible mounting angles of beam axes could be obtained. Lower limits corresponding to the maximum admissible mounting angles of beam axis in the inclined plane and area of typical mounting angles of beam axes in the vertical and horizontal planes are represented in Fig. 7 (Nekrasov, 2008b). Trace 1 and trace 2 are the lower limits corresponding to the maximum admissible mounting angles of beam axis in the inclined plane of 58.3° (lower limit of high accuracy of measurement at $\Delta f_D / F_D = 0.1$) and 72.9° (lower limit of sufficient high accuracy of measurement at $\Delta f_D / F_D = 0.2$),

respectively. A dash line displays the area of typical mounting angles of beam axes in the vertical and horizontal planes.

Fig. 7 demonstrates that for typical mounting angles of beam axes, sufficient high accuracy of measurement by the DNS is provided for the most part of the area of typical mounting angles in the vertical and horizontal planes. The measurement accuracy rises with increase of the beam incidence angle in the vertical plane.

The DNS multi-beam antenna allows selecting a power backscattered by the underlying surface from different directions, namely from directions corresponding to the appropriate beam relative to the aircraft course ψ, e.g. $\psi_{0.a.1}$, $\psi_{0.a.2}$, $\psi_{0.a.3}$, and $\psi_{0.a.4}$, as shown in Fig. 5. Each beam provides angular resolutions in the azimuthal and vertical planes, $\Delta\alpha$ and $\Delta\theta$ respectively. As three or four NRCS values obtained from considerably different azimuth directions are quite enough to measure the wind vector over water by intensity of reflected signal (Nekrassov, 1997), an airborne DNS can be used as a multi-beam (three- or four-beam) scatterometer for recovering the near-surface wind speed and direction. For this purpose, an airborne DNS having the following mounting angles of antenna beam axes $\theta_0 = 30^\circ$ and $\Gamma_0 = 30^\circ \div 45^\circ$, or $\theta_0 > 30^\circ$ ($\theta_0 \to 45^\circ$) and $\Gamma_0 = 30^\circ \div 45^\circ$, could be used. The second case requires a heightened transmitted power in comparison with the first case. Nevertheless, it allows a better usage the anisotropic properties of the water surface scattering at middle incidence angles to measure the near-surface wind vector, and also to increase an accuracy of measurement of typical DNS parameters.
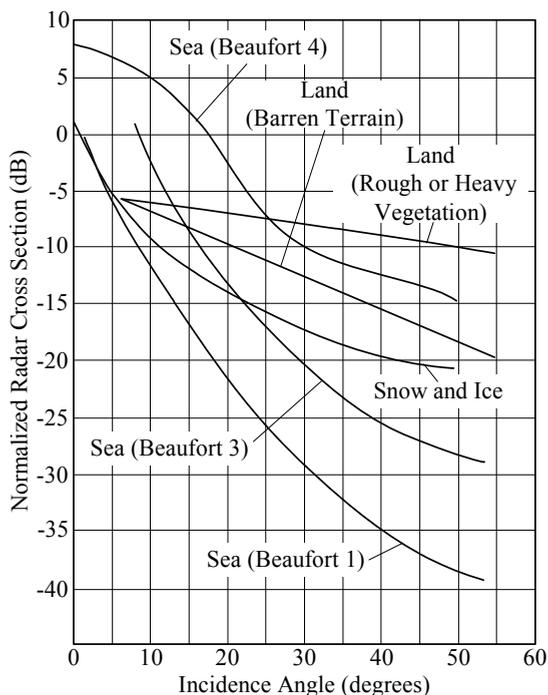

Fig. 6. Backscattering cross section per unit surface area (NRCS) versus incidence angle for different terrains at Ke-band (Kayton & Fried, 1997)
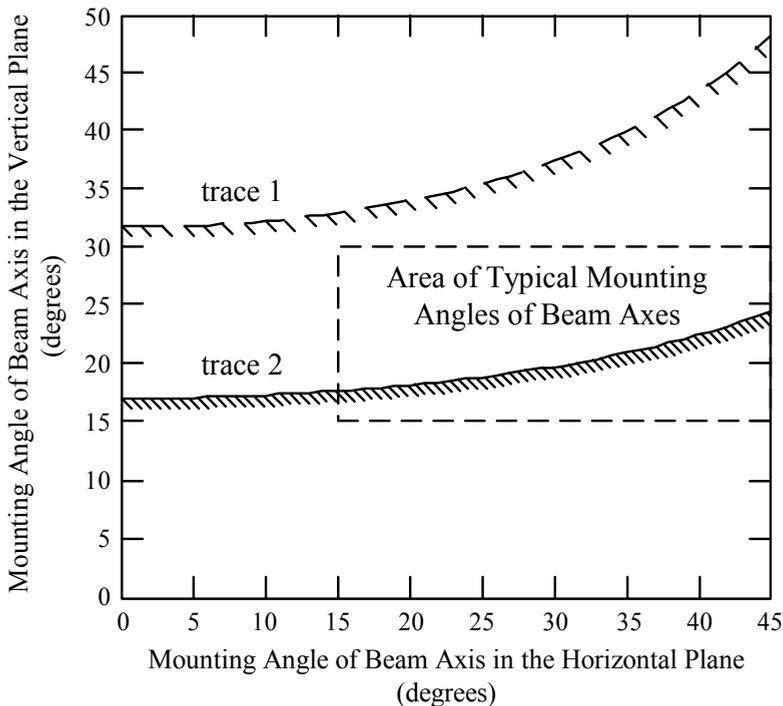
Fig. 7. Lower limits corresponding to the maximum admissible mounting angles of beam axis in the inclined plane and area of typical mounting angles of beam axes in the vertical and horizontal planes: trace 1 is the lower limit corresponding to the maximum admissible mounting angle of beam axis in the inclined plane of 58.3° (lower limit of high accuracy of measurement at $\Delta f_D / F_D = 0.1$); trace 2 is the lower limit, which corresponds to the maximum admissible mounting angle of beam axis in the inclined plane of 72.9° (lower limit of sufficient high accuracy of measurement at $\Delta f_D / F_D = 0.2$); dash line is the contour of the area of typical mounting angles of beam axes in the vertical and horizontal planes.

4.2 Wind Vector Estimation Using a Doppler Navigation System with the Fixed-Antenna System

Let a flying apparatus equipped with a DNS make a horizontal rectilinear flight with the speed V at some altitude H above the mean sea surface, the DNS use a multi-beam fixed-antenna system (physically non-stabilized to the local horizontal), and so, the values of the incidence angles of beams and beam locations in azimuthal plane are not equal to the chosen design values. Then, the actual azimuth direction of beam N $\psi_{\theta_{Y.a.N}}$ relative to the aircraft course (aircraft ground track) and the actual incidence angle of beam N $\theta_{\theta_{Y.a.N}}$ are

$$\psi_{\theta\gamma.a.N} = \begin{cases} \arctan\left(\dfrac{\tan(\arctan(\tan\theta_0\sin\psi_{0.a.N})+\gamma_{fa})}{\tan(\arctan(\tan\theta_0\cos\psi_{0.a.N})+\theta_{fa})}\right) \\ \quad \text{for} \quad \tan(\arctan(\tan\theta_0\cos\psi_{0.a.N})+\theta_{fa}) \geq 0, \\ \pi + \arctan\left(\dfrac{\tan(\arctan(\tan\theta_0\sin\psi_{0.a.N})+\gamma_{fa})}{\tan(\arctan(\tan\theta_0\cos\psi_{0.a.N})+\theta_{fa})}\right) \\ \quad \text{for} \quad \tan(\arctan(\tan\theta_0\cos\psi_{0.a.N})+\theta_{fa}) < 0, \end{cases} \tag{24}$$

$$\theta_{\theta\gamma.a.N} = \arctan\left(\sqrt{\tan^2(\arctan(\mathrm{tg}\theta_0\sin\psi_{0.a.N})+\gamma_{fa}) + } \right. \\ \left. \overrightarrow{} \overline{\tan^2(\arctan(\tan\theta_0\cos\psi_{0.a.N})+\theta_{fa})}\right), \tag{25}$$

where $\psi_{0.a.N}$ is the azimuthal mounting angle of the beam axis N relative to the aircraft course ψ, $\psi_{0.a.1}=\Gamma_0$, $\psi_{0.a.2}=180^\circ-\Gamma_0$, $\psi_{0.a.3}=180^\circ+\Gamma_0$, $\psi_{0.a.4}=360^\circ-\Gamma_0$, γ_{fa} is the roll angle of flying apparatus (right roll is positive), θ_{fa} is the pitch angle of flying apparatus (pull-up is positive).

For example, five-degree roll and pitch combinations at a mounting angle of a beam axis in the vertical plane of 30° and an arbitrary mounting angle of a beam axis in the azimuthal plane may lead to a beam axis shift up to 6.4° in the vertical plane and up to 14.4° in the azimuthal plane. The same roll and pitch combinations at a mounting angle of a beam axis in the vertical plane of 45° lead to a lesser beam axis shift up to 5.5° in the vertical plane and up to 10.6° in the azimuthal plane. So, that possible difference of the actual beam axis angles from the mounting angles should be taken into account under a measuring algorithm development, and it is desirable that the mounting angle of a beam axis in the vertical plane tends to 45°.

Let the sea surface wind blow in direction ψ_w, and the angle between the up-wind direction and the aircraft course is α. Let the NRCS model function for middle incident angles be of the form (1). In case of the selected cell is narrow enough in the vertical plane, that is true for the DNS, the NRCS model function for middle incidence angles (1) can be used without any correction for wind measurement while the azimuth angular size of a cell is up to $15^\circ - 20^\circ$ (Nekrassov, 1999). If the DNS would be a multi-beam roll-and-pitch-stabilized antenna system, the NRCS values obtained with beams 1, 2, 3 and 4 would be as fallows $\sigma^\circ(U,\theta_0,\alpha+\psi_{0.a.1})$, $\sigma^\circ(U,\theta_0,\alpha+\psi_{0.a.2})$, $\sigma^\circ(U,\theta_0,\alpha+\psi_{0.a.3})$ and $\sigma^\circ(U,\theta_0,\alpha+\psi_{0.a.4})$ respectively. As the DNS has a fixed-antenna system, the NRCS values obtained with beams 1, 2, 3 and 4 are $\sigma^\circ(U,\theta_{\theta\gamma.a.1},\alpha+\psi_{\theta\gamma.a.1})$, $\sigma^\circ(U,\theta_{\theta\gamma.a.2},\alpha+\psi_{\theta\gamma.a.2})$, $\sigma^\circ(U,\theta_{\theta\gamma.a.3},\alpha+\psi_{\theta\gamma.a.3})$ and $\sigma^\circ(U,\theta_{\theta\gamma.a.4},\alpha+\psi_{\theta\gamma.a.4})$ respectively. Then, the following algorithm to estimate the wind vector over the sea surface can be proposed.

The wind speed and up-wind direction are found by solving a system of equation for a three-beam DNS

$$
\begin{cases}
\sigma^\circ(U, \theta_{\theta\gamma.a.1}, \alpha + \psi_{\theta\gamma.a.1}) = A(U, \theta_{\theta\gamma.a.1}) + \\
\qquad\qquad B(U, \theta_{\theta\gamma.a.1})\cos(\alpha + \psi_{\theta\gamma.a.1}) + \\
\qquad\qquad C(U, \theta_{\theta\gamma.a.1})\cos(2(\alpha + \psi_{\theta\gamma.a.1})), \\
\sigma^\circ(U, \theta_{\theta\gamma.a.2}, \alpha + \psi_{\theta\gamma.a.2}) = A(U, \theta_{\theta\gamma.a.2}) + \\
\qquad\qquad B(U, \theta_{\theta\gamma.a.2})\cos(\alpha + \psi_{\theta\gamma.a.2}) + \\
\qquad\qquad C(U, \theta_{\theta\gamma.a.2})\cos(2(\alpha + \psi_{\theta\gamma.a.2})), \\
\sigma^\circ(U, \theta_{\theta\gamma.a.3}, \alpha + \psi_{\theta\gamma.a.3}) = A(U, \theta_{\theta\gamma.a.3}) + \\
\qquad\qquad B(U, \theta_{\theta\gamma.a.3})\cos(\alpha + \psi_{\theta\gamma.a.3}) + \\
\qquad\qquad C(U, \theta_{\theta\gamma.a.3})\cos(2(\alpha + \psi_{\theta\gamma.a.3})).
\end{cases}
\tag{26}
$$

and for a four-beam DNS (Nekrasov, 2008b)

$$
\begin{cases}
\sigma^\circ(U, \theta_{\theta\gamma.a.1}, \alpha + \psi_{\theta\gamma.a.1}) = A(U, \theta_{\theta\gamma.a.1}) + \\
\qquad\qquad B(U, \theta_{\theta\gamma.a.1})\cos(\alpha + \psi_{\theta\gamma.a.1}) + \\
\qquad\qquad C(U, \theta_{\theta\gamma.a.1})\cos(2(\alpha + \psi_{\theta\gamma.a.1})), \\
\sigma^\circ(U, \theta_{\theta\gamma.a.2}, \alpha + \psi_{\theta\gamma.a.2}) = A(U, \theta_{\theta\gamma.a.2}) + \\
\qquad\qquad B(U, \theta_{\theta\gamma.a.2})\cos(\alpha + \psi_{\theta\gamma.a.2}) + \\
\qquad\qquad C(U, \theta_{\theta\gamma.a.2})\cos(2(\alpha + \psi_{\theta\gamma.a.2})), \\
\sigma^\circ(U, \theta_{\theta\gamma.a.3}, \alpha + \psi_{\theta\gamma.a.3}) = A(U, \theta_{\theta\gamma.a.3}) + \\
\qquad\qquad B(U, \theta_{\theta\gamma.a.3})\cos(\alpha + \psi_{\theta\gamma.a.3}) + \\
\qquad\qquad C(U, \theta_{\theta\gamma.a.3})\cos(2(\alpha + \psi_{\theta\gamma.a.3})), \\
\sigma^\circ(U, \theta_{\theta\gamma.a.4}, \alpha + \psi_{\theta\gamma.a.4}) = A(U, \theta_{\theta\gamma.a.4}) + \\
\qquad\qquad B(U, \theta_{\theta\gamma.a.4})\cos(\alpha + \psi_{\theta\gamma.a.4}) + \\
\qquad\qquad C(U, \theta_{\theta\gamma.a.4})\cos(2(\alpha + \psi_{\theta\gamma.a.4})).
\end{cases}
\tag{27}
$$

Then, the wind direction can be found as follows

$$
\psi_w = \alpha \pm 180^\circ.
\tag{28}
$$

4.3 Wind Vector Estimation Using a Doppler Navigation System with the Roll-And-Pitch-Stabilized Antenna System

Let a flying apparatus equipped with a DNS make a horizontal rectilinear flight with the speed V at some altitude H above the mean sea surface, the DNS use a roll-and-pitch-stabilized antenna (physically stabilized to the local horizontal) and so the value of an incidence angle θ remains essentially constant and equal to the chosen design value θ_0. Let the aircraft velocity vector V be located along the intersection of the local horizontal plane and the local vertical plane through the longitudinal axis of aircraft (condition of no-drift angle and no-climb angle), that means that the aircraft flight is horizontal and the aircraft course ψ is the same as the aircraft's ground track. The directions of the DNS beams 1, 2, 3, 4

relative to the aircraft course are $\psi_{0.a.1}$, $\psi_{0.a.2}$, $\psi_{0.a.3}$, and $\psi_{0.a.4}$, respectively (Fig. 5.). Let the sea surface wind blow in direction ψ_w, and the angle between the up-wind direction and the aircraft course is α. Let the NRCS model function for middle incident angles be of the form (1). Then, the NRCS values obtained with beams 1, 2, 3, 4 are $\sigma^\circ(U, \theta_0, \alpha + \psi_{0.a.1})$, $\sigma^\circ(U, \theta_0, \alpha + \psi_{0.a.2})$, $\sigma^\circ(U, \theta_0, \alpha + \psi_{0.a.3})$ and $\sigma^\circ(U, \theta_0, \alpha + \psi_{0.a.4})$ respectively, and the wind speed and up-wind direction are found by solving a system of equation (26) for a three-beam DNS, or (27) for a four-beam DNS. Then, the wind direction can be found from (28).

Let a mounting angle of a beam axis in the horizontal plane is equal to 45°. As the DNS antenna is roll-and-pitch-stabilized, the directions of the DNS beams remains constant, and the NRCS values obtained with beams 1, 2, 3, 4 are $\sigma^\circ(U, \theta_0, \alpha + 45^\circ)$, $\sigma^\circ(U, \theta_0, \alpha + 135^\circ)$, $\sigma^\circ(U, \theta, \alpha + 225^\circ)$, $\sigma^\circ(U, \theta_0, \alpha + 315^\circ)$. Then, the following algorithm to estimate the wind vector over the sea surface can be proposed.

The wind speed can be found from the following equation (Nekrasov, 2005)

$$
U = \left(\frac{A(U, \theta_0)}{a_0(\theta_0)} \right)^{1/\gamma_0(\theta_0)} =
$$

$$
\left(\frac{\sigma^\circ(U, \theta_0, \alpha + 45^\circ) + \sigma^\circ(U, \theta_0, \alpha + 135^\circ) +}{4 a_0(\theta_0)} \right. \rightarrow
$$

$$
\left. \frac{\sigma^\circ(U, \theta_0, \alpha + 225^\circ) + \sigma^\circ(U, \theta_0, \alpha + 315^\circ)}{} \right)^{1/\gamma_0(\theta_0)} . \tag{29}
$$

To find the wind direction, at first, the space of possible solutions could be divided into four quadrants. The quadrant, which contains the solution, should be found, and then, the unique wind direction can be obtained as follows

$$
\textit{if } \sigma^\circ(U, \theta_0, \alpha + 45^\circ) > \sigma^\circ(U, \theta_0, \alpha + 225^\circ)
$$

$$
\textit{and } \sigma^\circ(U, \theta_0, \alpha + 135^\circ) \geq \sigma^\circ(U, \theta_0, \alpha + 315^\circ) \Rightarrow \psi_w = \psi + 45^\circ + \alpha_q \pm 180^\circ,
$$

$$
\textit{if } \sigma^\circ(U, \theta_0, \alpha + 45^\circ) \leq \sigma^\circ(U, \theta_0, \alpha + 225^\circ)
$$

$$
\textit{and } \sigma^\circ(U, \theta_0, \alpha + 135^\circ) > \sigma^\circ(U, \theta_0, \alpha + 315^\circ) \Rightarrow \psi_w = \psi + 225^\circ - \alpha_q \pm 180^\circ,
$$

$$
\textit{if } \sigma^\circ(U, \theta_0, \alpha + 45^\circ) < \sigma^\circ(U, \theta_0, \alpha + 225^\circ)
$$

$$
\textit{and } \sigma^\circ(U, \theta_0, \alpha + 135^\circ) \leq \sigma^\circ(U, \theta_0, \alpha + 315^\circ) \Rightarrow \psi_w = \psi + 225^\circ + \alpha_q \pm 180^\circ,
$$

$$
\textit{if } \sigma^\circ(U, \theta_0, \alpha + 45^\circ) \geq \sigma^\circ(U, \theta_0, \alpha + 225^\circ)
$$

$$
\textit{and } \sigma^\circ(U, \theta_0, \alpha + 135^\circ) < \sigma^\circ(U, \theta_0, \alpha + 315^\circ) \Rightarrow \psi_w = \psi + 45^\circ - \alpha_q \pm 180^\circ, \tag{30}
$$

where α_q is the angle of the wind in the quadrant,

$$\alpha_q = \begin{cases} 0^\circ, & A_1 \geq 1 \\ 0.5\arccos A_1, & -1 < A_1 < 1 \\ 90^\circ, & A_1 \leq 1 \end{cases}$$ (31)

$$A_1 = \frac{\sigma^\circ(U,\theta_0,\alpha+45^\circ) + \sigma^\circ(U,\theta_0,\alpha+225^\circ) - 2A(U,\theta_0)}{2C(U,\theta_0)}.$$ (32)

4.4 Conclusion to Wind Vector Estimation Using a Doppler Navigation System

The analysis of the DNS, the backscatter model function and the geometry of wind vector measurements have shown that the wind vector over sea can be measured by an airborne DNS that has three- or four-beam fixed or roll-and-pitch-stabilized antenna system and employed as a multi-beam scatterometer.

For this purpose, an airborne DNS having the following mounting angles of antenna beam axes $\theta_0 = 30^\circ$ and $\Gamma_0 = 30^\circ \div 45^\circ$, or $\theta_0 > 30^\circ$ ($\theta_0 \to 45^\circ$) and $\Gamma_0 = 30^\circ \div 45^\circ$, could be used.

The second case requires a heightened transmitted power in comparison with the first case. Nevertheless, it allows a better usage the anisotropic properties of the water surface scattering at middle incidence angles to measure the near-surface wind vector, to increase an accuracy of measurement of typical DNS parameters, and also to decrease a beam axis deviation due to roll and pitch influence.

5. Measuring the Wind Vector by an Airborne Weather Radar

5.1 Airborne Weather Radar

AWR is radar equipment mounted on an aircraft for purposes of weather observation and avoidance, aircraft position finding relative to landmarks, and drift angle measuring (Sosnovsky, et al, 1990). The AWR is necessary equipment of any civil airplane. It must be obligatory installed on all civil airliners. All military transport aircrafts are usually equipped by weather radars too. Due to the specificity of airborne application, designers of avionics systems always try to use the most efficient progressive methods and reliable engineering solutions that provide flight safety and flight regularity at harsh environment (Yanovsky, 2005).

The development of the AWR is mainly associated with growing functionalities on detection of different dangerous weather phenomena. The radar observations involved in a weather mode are magnitude detection of reflections from clouds and precipitation and Doppler measurements of the motion of particles within a weather formation. Magnitude detection allows determination of particle type (rain, snow, hail, etc.) and precipitation rate. Doppler measurements can be made to yield estimates of turbulence intensity and wind speed. Reliable determination of the presence and severity of the phenomenon known as wind shear is an important area of study too (Kayton & Fried, 1997).

Nevertheless, the second important assignment of the AWR is providing a pilot with navigation information using earth surface mapping. In this case a possibility to extract some navigation information that allows determining aircraft position with respect to a geographic map is very important for air navigation. Landmark's coordinates relative to the

airplane that are measured by the AWR give a possibility to set flight computer for exacter and more efficient fulfilment of en-route flight, cargo delivery, and cargo throw down to the given point. These improve tactical possibilities of transport aircraft, airplanes of search-and-rescue service, and local airways (Yanovsky, 2005).

Other specific function of the AWR is interaction with ground-based responder beacons. New functions of the airborne weather radar are detection and visualization of runways at approach landing as well as visualization of taxiways and obstacles on the taxiway at taxiing.

Certainly, not all of the mentioned functions are implemented in a particular airborne radar system. Nevertheless, the airborne weather radar always is a multifunctional system that provides earth surface surveillance and weather observation. Usually, weather radar should at least enable to detect clouds and precipitation, select zones of meteorological danger, and show radar image of surface in the map mode.

AWRs or multimode radars with a weather mode are usually nose mounted. Most AWRs operate in either X- or C-band (Kayton & Fried, 1997). The λ^{-4} dependence of weather formations on carrier wavelength λ favours X-band radar for their detecting. At the same time, the X-band provides the performance of the long-range weather mode better than Ku-band. The AWR antenna, in the ground-mapping mode, has a large cosecant-squared elevation beam where horizontal dimension is narrow (2° to 6°) while the other is relatively broad (10° to 30°), and it sweeps in an azimuth sector (up to ±100°) (Kayton & Fried, 1997), (Sosnovskiy & Khaymovich, 1987). The scan plane is horizontal because of the antenna is stabilized (roll-and-pitch-stabilized). Those features allow supposing that the AWR in the ground-mapping mode can be also used as a scatterometer for the wind speed and direction retrieval over water.

5.2 Wind Vector Estimation Using an Airborne Weather Radar Having a Narrow Scanning Sector

Let a flying apparatus equipped with an AWR make a horizontal rectilinear flight with the speed V at some altitude H above the mean sea surface, an AWR operate in the ground-mapping mode as a scatterometer, the radar antenna have different beamwidth in the vertical $\theta_{a.v}$ and horizontal $\theta_{a.h}$ planes ($\theta_{a.v} > \theta_{a.h}$) as shown in Fig. 8, and scan periodically through an azimuth in a narrow sector (narrower than ±90° but no narrower than ±45°) as shown in Fig. 9. Also let a delay selection be used to provide a necessary resolution in the vertical plane.

Then, the beam scanning allows selecting a power backscattered by the underlying surface for given incidence angle θ from various directions in an azimuth sector, e.g. from directions $\alpha - 45°$, α and $\alpha + 45°$ relative to the up-wind direction as represented in Fig. 9. Angular (narrow horizontal beamwidth) selection in the horizontal plane along with the delay selection provide angular resolutions in the azimuthal and vertical planes, $\Delta\alpha$ and $\Delta\theta$ respectively. As three or four NRCS values obtained from considerably different azimuth directions are quite enough to measure the wind vector over water by intensity of reflected signal (Nekrassov, 1997), AWR can be used as a scanning scatterometer for recovering the near-surface wind speed and direction.
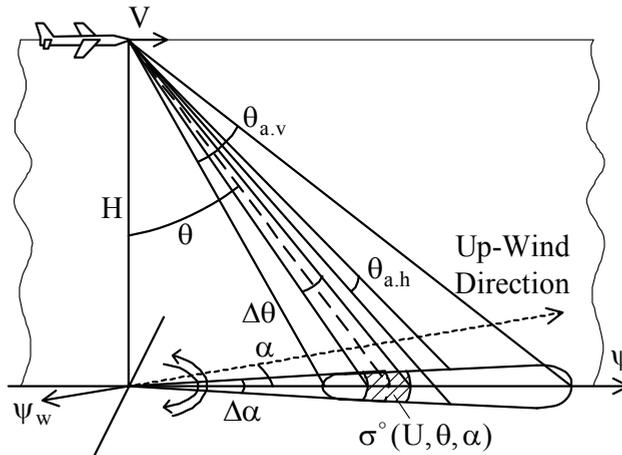
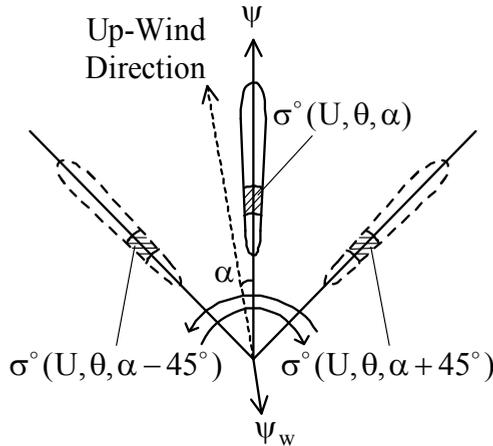Fig. 8. Airborne weather radar beam and selected cell geometry

Fig. 9. Scanning beam footprints in a narrow sector and selected cells

Let the sea surface wind blow in direction ψ_w, and the angle between the up-wind direction and the aircraft course ψ is α. Let the NRCS model function for middle incident angles be of the form (1). In case of the selected cell is narrow enough in the vertical plane, the NRCS model function for middle incidence angles (1) can be used without any correction for wind measurement while the azimuth angular size of a cell is up to $15^\circ - 20^\circ$ (Nekrassov, 1999).

Let the NRCS values be obtained only from directions $\alpha - 45^\circ$, α and $\alpha + 45^\circ$. They are $\sigma^\circ(U, \theta, \alpha - 45^\circ)$, $\sigma^\circ(U, \theta, \alpha)$, and $\sigma^\circ(U, \theta, \alpha + 45^\circ)$ respectively. Then, the following algorithm to estimate the wind vector over the sea surface can be proposed.

The wind speed and up-wind direction are found by solving the following system of equations (Nekrasov & Labun 2008)

$$\begin{cases} \sigma°(U,\theta,\alpha-45°) = A(U,\theta) + B(U,\theta)\cos(\alpha-45°) + \\ \qquad\qquad C(U,\theta)\cos(2(\alpha-45°)), \\ \sigma°(U,\theta,\alpha) = A(U,\theta) + B(U,\theta)\cos\alpha + \\ \qquad\qquad C(U,\theta)\cos(2\alpha)), \\ \sigma°(U,\theta,\alpha+45°) = A(U,\theta) + B(U,\theta)\cos(\alpha+45°) + \\ \qquad\qquad C(U,\theta)\cos(2(\alpha+45°)). \end{cases} \qquad (33)$$

The system of equations (33) could be solved approximately using searching procedure within the ranges of discrete values of possible solutions. Then, the wind direction can be found from (28).

It is necessary to note that the AWR in the mode of the wind vector measurement should use the horizontal transmit and receive polarization, and provide the incidence angle of the selected sells $\theta \to 45°$ that is explained by better usage of the anisotropic properties of the water surface scattering at middle incidence angles and also by power reasons. For water surfaces, the NRCS falls radically as the incidence angle increases and assumes different values for different conditions of sea state or water roughness while, for most other types of terrain, the NRCS decreases slowly with increase of the beam incidence angle (Kayton & Fried, 1997). Or at least, the incidence angle of the selected sells should be in the range of validity for the NRCS model function (1), and should be out of the "shadow" region.

5.2 Wind Vector Estimation Using an Airborne Weather Radar Having a Wide Scanning Sector

Let a flying apparatus equipped with an AWR make a horizontal rectilinear flight with the speed V at some altitude H above the mean sea surface, the AWR operate in the ground-mapping mode as a scatterometer, the radar antenna have different beamwidth in the vertical $\theta_{a.v}$ and horizontal $\theta_{a.h}$ planes ($\theta_{a.v} > \theta_{a.h}$) as shown in Fig. 8, and scan periodically through an azimuth in a sector of ±90° or wider as shown in Fig. 10. Also let a delay selection be used to provide a necessary resolution in the vertical plane.
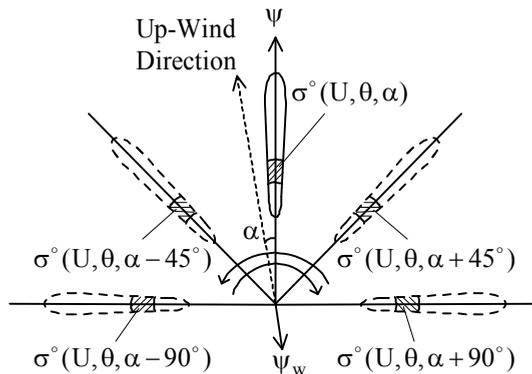

Fig. 10. Scanning beam footprints in a wide sector and selected cells

Then, the beam scanning allows selecting a power backscattered by the underlying surface for given incidence angle θ from various directions in an azimuth sector, e.g. from directions $\alpha - 90°$, $\alpha - 45°$, α, $\alpha + 45°$, and $\alpha + 90°$ relative to the up-wind direction as represented in Fig. 10. Angular (narrow horizontal beamwidth) selection in the horizontal plane along with the delay selection provide angular resolutions in the azimuthal and vertical planes, $\Delta\alpha$ and $\Delta\theta$ respectively.

Let the sea surface wind blow in direction ψ_w, and the angle between the up-wind direction and the aircraft course ψ is α, and the NRCS values be obtained only from directions $\alpha - 90°$, $\alpha - 45°$, α, $\alpha + 45°$, and $\alpha + 90°$. They are $\sigma°(U,\theta,\alpha-90°)$ $\sigma°(U,\theta,\alpha-45°)$, $\sigma°(U,\theta,\alpha)$, $\sigma°(U,\theta,\alpha+45°)$, and $\sigma°(U,\theta,\alpha+90°)$ respectively. Then, the following algorithm to estimate the wind vector over the sea surface can be proposed.

Using the measuring geometry, equation (1), and taking into account that the azimuth angular size of the selected sells are narrow enough, the following system of equations can be written down (Nekrasov, 2009)

$$
\begin{cases}
\sigma°(U,\theta,\alpha-90°) = A(U,\theta) + B(U,\theta)\cos(\alpha-90°) + \\
\qquad\qquad C(U,\theta)\cos(2(\alpha-90°)), \\
\sigma°(U,\theta,\alpha-45°) = A(U,\theta) + B(U,\theta)\cos(\alpha-45°) + \\
\qquad\qquad C(U,\theta)\cos(2(\alpha-45°)), \\
\sigma°(U,\theta,\alpha) = A(U,\theta) + B(U,\theta)\cos\alpha + C(U,\theta)\cos(2\alpha)), \\
\sigma°(U,\theta,\alpha+45°) = A(U,\theta) + B(U,\theta)\cos(\alpha+45°) + \\
\qquad\qquad C(U,\theta)\cos(2(\alpha+45°)), \\
\sigma°(U,\theta,\alpha+90°) = A(U,\theta) + B(U,\theta)\cos(\alpha+90°) + \\
\qquad\qquad C(U,\theta)\cos(2(\alpha+90°)).
\end{cases}
\tag{34}
$$

From the sum of the first and the fifth equations of (34) we have

$$
\cos 2\alpha = \frac{\sigma°(U,\theta,\alpha-90°) + \sigma°(U,\theta,\alpha+90°) - 2A(U,\theta)}{2C(U,\theta)} .
\tag{35}
$$

From the sum of the second and the fourth equations of (34) we obtain

$$
\cos\alpha = \frac{\sigma°(U,\theta,\alpha-45°) + \sigma°(U,\theta,\alpha+45°) - 2A(U,\theta)}{\sqrt{2}B(U,\theta)} .
\tag{36}
$$

Substitution of cos2α from (35) and cosα from (36) into the third equation of system (34) gives the following equation

$$A(U,\theta) = \frac{1}{\sqrt{2}}\sigma^{\circ}(U,\theta,\alpha) - \frac{1}{2}\Big(\sigma^{\circ}(U,\theta,\alpha-45^{\circ}) + \sigma^{\circ}(U,\theta,\alpha+45^{\circ})\Big) -$$
$$\frac{1}{2\sqrt{2}}\Big(\sigma^{\circ}(U,\theta,\alpha-90^{\circ}) + \sigma^{\circ}(U,\theta,\alpha+90^{\circ})\Big). \tag{37}$$

The wind speed over water can be calculated from (37). Then, two possible up-wind directions relative the course of the flying apparatus can be found from (36). They are

$$\alpha_{1,2} = \pm\arccos\left(\frac{\sigma^{\circ}(U,\theta,\alpha-45^{\circ}) + \sigma^{\circ}(U,\theta,\alpha+45^{\circ}) - 2A(U,\theta)}{\sqrt{2}B(U,\theta)}\right). \tag{38}$$

The unique up-wind direction α relative the course can be found by substitution of the values α_1 and α_2 into the first and the fifth equations of the system of equations (34). Finally, the wind direction ψ_w can be found from (18).

5.4 Conclusion to Wind Vector Estimation Using an Airborne Weather Radar

The analysis of the AWR, the backscatter model function and the geometry of wind vector measurements have shown that the wind vector over sea can be measured by an AWR employed in the ground-mapping mode as a scatterometer scanning periodically through an azimuth in a narrow sector (narrower than ±90° but no narrower than ±45°) and a wide sector (±90° or wider), in addition to its typical meteorological and navigation application.

The AWR in the mode of the wind vector measurement should use the horizontal transmit and receive polarization, and provide the incidence angle of the selected sells $\theta \rightarrow 45^{\circ}$ that is explained by better usage of the anisotropic properties of the water surface scattering at middle incidence angles and also by power reasons. Or at least, the incidence angle of the selected sells should be in the range of validity for the NRCS model function (1), and should be out of the "shadow" region.

6. Conclusion

The study has shown that the ARA, DNS and AWR can be used as measuring instruments for the wind vector over water in addition to their typical navigation applications. The ARA should be employed as a nadir-looking wide-beam short-pulse scatterometer in conjunction with Doppler filtering. The DNS having the three- or four-beam fixed or roll-and-pitch-stabilized antenna system should be used as a multi-beam scatterometer. The AWR may be employed in the ground-mapping mode as a scatterometer scanning periodically through an azimuth in the narrow or wide sector.

As no commercial equipment exists so far, the results obtained can be used for creation of a new airborne radar system for stand-alone and simultaneous measurements of the water surface backscattering signature and the wind vector over water, including applications to amphibian aircraft safe landing on the water surface, in particular under search and rescue missions or fire-fighting operations in the fire risk coastal areas that could help to save the human lives and environment.

7. Acknowledgment

8. References

Carswell, J.R.; Carson, S.C.; McIntosh, R.E.; Li, F.K.; Neumann, G.; McLaughlin, D.J.; Wilkerson, J.C.; Black, P.G. & Nghiem, S.V. (1994) Airborne scatterometers: Investigating ocean backscatter under low- and high-wind conditions, *Proceedings of the IEEE*, Vol. 82, No. 12, pp. 1835–1860.

Chelton, D.B. & McCabe, P.J. (1985) A review of satellite altimeter measurement of sea surface wind speed: With a proposed new algorithm, *Journal of Geophysical Research*, Vol. 90, No. C3, pp. 4707–4720.

Davydov, P.S.; Zhavoronkov, V.P.; Kashcheyev, G.V.; Krinitsyn, V.V.; Uvarov, V.S. & Khresin, I.N. (1977) *Radar Systems of Flying Apparatuses*, Transport, Moscow, 352 p., *in Russian*.

Du, Y.; Vachon, P.W. & Wolf, J. (2002) Wind direction estimation from SAR images of the ocean using wavelet analysis, *Canadian Journal of Remote Sensing*, Vol. 28, No. 3, pp. 498–509.

Feindt, F.; Wismann, V.; Alpers, W. & Keller, W.C. (1986) Airborne measurements of the ocean radar cross section at 5.3 GHz as a function of wind speed, *Radio Science*, Vol. 21, No. 5, pp. 845–856.

Hammond, D.L.; Mennella, R.A., & Walsh, E.J. (1977) Short pulse radar used to measure sea surface wind speed and SWH, *IEEE Transactions on Antennas and Propagation*, Vol. 25, No. 1, pp. 61–67.

Hildebrand, P.H. (1994) Estimation of sea-surface wind using backscatter cross-section measurements from airborne research weather radar, *IEEE Transactions on Geoscience and Remote Sensing*, Vol. 32, No. 1, pp. 110–117.

Jackson, F.C.; Walton, W.T.; Hines, D.E.; Walter, B.A. & Peng, C.Y. (1992) Sea surface mean square slope from K_u-band backscatter data, *Journal of Geophysical Research*, Vol. 97, No. C7, pp. 11411–11427.

Kayton M. & Fried W.R. (1997) *Avionics Navigation Systems*, John Wieley & Sons, New York, 773 p.

Kolchinskiy, V.Ye.; Mandurovskiy, I.A. & Konstantinovskiy, M.I. (1975) *Autonomous Doppler Facilities and Systems for Navigation of Flying Apparatuses,* Sovetskoye Radio, Moscow, 432 p., *in Russian*.

Komen, G.J.; Cavaleri, L.; Donelan, M.; Hasselmann, K.; Hasselmann, S. & Janssen, P.A.E.M. (1994) *Dynamics and Modelling of Ocean Waves,* Cambridge University Press, Cambridge, 532 p.

Komjathy, A.; Armatys, M.; Masters, D.; Axelrad, P.; Zavorotny, V.U. & Katzberg, S.J. (2001) Developments in using GPS for oceanographic remote sensing: Retrieval of ocean surface wind speed and wind direction, *CD Proceedings of the ION National Technical Meeting*, Long Beach, CA, USA, 9 p.

Komjathy, A.; Zavorotny, V.; Axelrad, P.; Born, G. & Garrison, J.L. (2000) GPS signal scattering from sea surface: Wind speed retrieval using experimental data and theoretical model, *Remote Sensing of Environment*, Vol. 73, No. 2, pp. 162–174.

Long, D.G.; Donelan, M.A.; Freilich, M.H.; Graber, H.C.; Masuko, H.; Pierson, W.J.; Plant, W.J.; Weissman, D. & Wentz, F. (1996) Current progress in Ku-band model functions, Brigham Young Univ., USA, Tech. Rep. MERS 96-002, 88 p.

Masuko, H.; Okamoto, K.; Shimada M. & Niwa, S. (1986) Measurement of microwave backscattering signatures of the ocean surface using X band and Ka band airborne scatterometers, *Journal of Geophysical Research*, Vol. 91, No. C11, pp. 13065–13083.

Melnik, Yu.A. (1980) *Radar Methods of the Earth Exploration*, Sovetskoye Radio, Moscow, 264 p., *in Russian*.

Moore, R.K. & Fung, A.K. (1979) Radar determination of winds at sea, *Proceedings of the IEEE*, Vol. 67, No. 11, pp. 1504–1521.

Nekrasov, A. (2005) On possibility to measure the sea surface wind vector by the Doppler navigation system of flying apparatus. *Proceedings of RADAR 2005*, Arlington, Virginia, USA, pp. 747-752.

Nekrasov, A. (2007) Measurement of the wind vector over sea by an airborne radar altimeter, which has an antenna with the ellipse beam shape, *Proceedings of APMC 2007*, Bangkok, Thailand, pp. 91-94.

Nekrasov, A. (2008a) Measurement of the wind vector over sea by an airborne radar altimeter having an antenna with the different beamwidth in the vertical and horizontal planes, *IEEE Geoscience and Remote Sensing Letters*, Vol. 5, No. 1, pp. 31-33.

Nekrasov, A. (2008b) Measuring the sea surface wind vector by the Doppler navigation system of flying apparatus that has a four-beam fixed-antenna system, *Proceedings of RADAR 2008*, Adelaide, Australia, pp. 493-498.

Nekrasov, A. (2009) Measurement of the sea surface wind vector by the airborne weather radar having a wide scanning sector, *Accepted to Radar 2009*, Bordeaux, France, 4 p.

Nekrasov, A. & Labun, J. (2008) About measurement of the sea surface wind vector by the airborne weather radar, *Acta Avionica*, Vol. X, No. 16, pp. 98-103.

Nekrassov, A. (1997) Measurement of sea surface wind speed and its navigational direction from flying apparatus, *Proceedings of Oceans'97*, Halifax, Nova Scotia, Canada, pp. 83–86.

Nekrassov, A. (1999) Sea surface wind vector measurement by airborne scatterometer having wide-beam antenna in horizontal plane, *Proceedings of IGARSS'99*, Hamburg, Germany, Vol. 2, pp. 1001–1003.

Nekrassov, A. (2001) Measurement of the sea surface wind speed and direction by an airborne microwave radar altimeter, GKSS Report No. GKSS/2001/38, Geesthacht, Germany, 17 p.

Nekrassov, A. (2002) On airborne measurement of the sea surface wind vector by a scatterometer (altimeter) with a nadir-looking wide-beam antenna, *IEEE Transactions on Geoscience and Remote Sensing*, Vol. 40, No. 10, pp. 2111-2116.

Nekrassov, A. (2003) Airborne measurement of the sea surface wind vector by a microwave radar altimeter at low speed of flight, *IEICE Transactions on Electronics*, Vol. E86-C, No. 8, pp. 1572-1579.

Raney, R.K. (1998) The delay/Doppler radar altimeter, *IEEE Transactions on Geoscience and Remote Sensing*, Vol. 36, No. 5, pp. 1578–1588.

Romeiser, R.; Schmidt, A. & Alpers, W. (1994) A three-scale composite surface model for the ocean wave-radar modulation transfer function, *Journal of Geophysical Research*, Vol. 99, No. C5, pp. 9785–9801.

Schöne, T. & Eickschen, S. (2000) Wind speed and SWH calibration for radar altimetry in the North Sea, *CD Proceedings of the ERS-Envisat Symposium*, Gothenburg, Sweden, p. 8.

Sosnovskiy, A.A. & Khaymovich, I.A. (1987) *Radio-Electronic Equipment of Flying Apparatuses*, Transport, Moscow, 256 p., *in Russian*.

Sosnovsky, A.A.; Khaymovich, I.A.; Lutin, E.A. & Maximov, I.B. (1990) *Aviation Radio Navigation: Handbook*, Transport, Moscow, 264 p., *in Russian*.

Spencer, M.W. & Graf, J.E. (1997) The NASA scatterometer (NSCAT) mission, *Backscatter*, Vol. 8, No. 4, pp. 18–24.

Spencer, W.M.; Tsai, W.-Y. & Long, D.G. (2000a) High resolution scatterometry by simultaneous range/Doppler discrimination, *Proceedings of IGARSS 2000*, Honolulu, Hawaii, USA, pp. 3166–3168.

Spencer, W.M.; Wu, C. & Long, D.G. (2000b) Improved resolution backscatter measurements with the SeaWinds pencil-beam scatterometer, *IEEE Transactions on Geoscience and Remote Sensing*, Vol. 38, No. 1, pp. 89–104.

Ulaby, F.T.; Moore, R.K. & Fung, A.K. (1982) *Microwave Remote Sensing: Active and Pasive*, Volume 2: *Radar Remote Sensing and Surface Scattering and Emission Theory*, Addison-Wesley, London, 1064 p.

Wackerman, C.C.; Rufenach, C.L.; Shuchman, R.A.; Johannessen, J.A. & Davidson, K.L. (1996) Wind vector retrieval using ERS-1 synthetic aperture radar imagery, *IEEE Transactions on Geoscience and Remote Sensing*, Vol. 34, No. 6, pp. 1343–1352.

Wentz, F.J.; Peteherych, S. & Thomas, L.A. (1984) A model function for ocean radar cross sections at 14.6 GHz, *Journal of Geophysical Research*, Vol. 89, No. C5, pp. 3689-3704.

Wismann, V. (1989) Messung der Windgeschwindigkeit über dem Meer mit einem flugzeuggetragenen 5.3 GHz Scatterometer, Dissertation zur Erlangung des Grades eines Doktors der Naturwissenschaften, Universität Bremen, Bremen, Germany, 119 S.

Yanovsky, F.J. (2005) Evolution and prospects of airborne weather radar functionality and technology, *Proceedings of ICECom 2005*, Dubrovnik, Croatia, pp. 1–4.

Young, I.R. (1993) An estimate of the Geosat altimeter wind speed algorithm at high wind speeds, *Journal of Geophysical Research*, Vol. 98, No. C11, pp. 20275–20285.
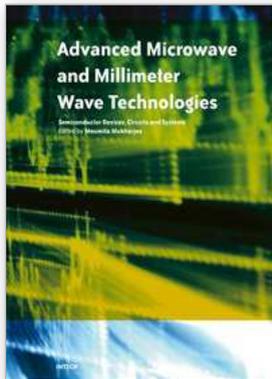
Advanced Microwave and Millimeter Wave Technologies
Semiconductor Devices Circuits and Systems
Edited by Moumita Mukherjee

This book is planned to publish with an objective to provide a state-of-the-art reference book in the areas of advanced microwave, MM-Wave and THz devices, antennas and systemtechnologies for microwave communication engineers, Scientists and post-graduate students of electrical and electronics engineering, applied physicists. This reference book is a collection of 30 Chapters characterized in 3 parts: Advanced Microwave and MM-wave devices, integrated microwave and MM-wave circuits and Antennas and advanced microwave computer techniques, focusing on simulation, theories and applications. This book provides a comprehensive overview of the components and devices used in microwave and MM-Wave circuits, including microwave transmission lines, resonators, filters, ferrite devices, solid state devices, transistor oscillators and amplifiers, directional couplers, microstripeline components, microwave detectors, mixers, converters and harmonic generators, and microwave solid-state switches, phase shifters and attenuators. Several applications area also discusses here, like consumer, industrial, biomedical, and chemical applications of microwave technology. It also covers microwave instrumentation and measurement, thermodynamics, and applications in navigation and radio communication.

How to reference
In order to correctly reference this scholarly work, feel free to copy and paste the following: